

Title: **Measuring Residual Stress and the
Resulting Stress Intensity Factor in
Compact Tension Specimens**

Author(s): **M. B. Prime**

Submitted to: **Fatigue & Fracture of Engineering
Materials & Structures
Volume 22
Number 3, March 1999
pp. 195-204**

Los Alamos
NATIONAL LABORATORY

Los Alamos National Laboratory, an affirmative action/equal opportunity employer, is operated by the University of California for the U.S. Department of Energy under contract W-7405-ENG-36. By acceptance of this article, the publisher recognizes that the U.S. Government retains a nonexclusive, royalty-free license to publish or reproduce the published form of this contribution, or to allow others to do so, for U.S. Government purposes. Los Alamos National Laboratory requests that the publisher identify this article as work performed under the auspices of the U.S. Department of Energy. The Los Alamos National Laboratory strongly supports academic freedom and a researcher's right to publish; as an institution, however, the Laboratory does not endorse the viewpoint of a publication or guarantee its technical correctness.

MEASURING RESIDUAL STRESS AND THE RESULTING STRESS INTENSITY FACTOR IN COMPACT TENSION SPECIMENS

M. B. Prime

prime@lanl.gov

Engineering Sciences & Applications Division
Los Alamos National Laboratory, Los Alamos, NM 87545, USA

ABSTRACT

The measurement of residual stress through the remaining ligament of a compact tension specimen was studied. In the crack compliance method, a slot or notch is successively extended through the part, and the resulting strain is measured at an appropriate location. By using a finite element simulation of a specimen preloaded beyond yield, three techniques for determining the original residual stress from the measured strains were compared for accuracy and sensitivity to measurement errors. A common beam-bending approximation was substantially inaccurate. The series expansion method proved to be very versatile and accurate. The fracture mechanics approach could determine the stress intensity factor caused by the residual stresses with a very simple calculation. This approach offers the exciting possibility of determining the stress intensity factor prior to a fatigue or fracture test by measuring strains during the specimen preparation.

KEYWORDS

residual stress; crack compliance; compact tension specimen; fracture mechanics; weight function; fatigue.

NOMENCLATURE

a	=	crack or slot length
a_0	=	initial crack or slot length
A_i	=	coefficients in stress series expansion
B	=	specimen out-of-plane thickness
C_i	=	compliances
CT	=	compact tension
E	=	elastic modulus
h	=	fracture mechanics weight function
K_I	=	mode I stress intensity factor
P_i	=	terms in stress series expansion
W	=	size of compact tension specimen
Z	=	influence function
ε	=	strain ($\mu\varepsilon$ is microstrain – $10^{-6} \varepsilon$)
ν	=	Poisson's ratio
σ	=	stress

INTRODUCTION

Residual stresses play a key role in fatigue crack growth, crack closure, and fracture. Although residual stresses affect only the mean stress, or stress ratio, in fatigue, these have been shown to influence crack initiation, propagation, and closure [e.g., 1–6]. Even under purely compressive far-field loading, fatigue cracks can initiate and propagate because of tensile residual stress [e.g., 7–9]. Knowledge of residual stresses is crucial both for correct interpretation of laboratory fatigue crack growth experiments and for prediction of service failures. To be more specific, the resulting stress intensity factor is often of greater interest than the residual stresses themselves because it appears directly in the fatigue crack growth and fracture relations.

Reid developed a simple technique for measuring residual stress in a compact tension (CT) specimen [10] that is, unfortunately, unacceptably inaccurate. In this technique, the notch is successively extended while the strain changes on the back face of the specimen are recorded. The technique is simple, requires only commonly available equipment, and has been applied several times to CT specimens [11–13]. However, the analysis relies on a beam-bending approximation that this study demonstrates to be significantly inaccurate.

The technique of successive slot extension to measure residual stress has been extensively developed as the crack compliance method [e.g., 14, review in 15]. Although the analysis used is versatile and more accurate than Reid's, it requires extensive computation. Recently, Schindler et al. developed a potentially simpler variation of the analysis, which uses fracture mechanics relations [16,17]. Although previous researchers

have used stress intensity factor (K_I) weight functions in their analyses [e.g., 18], only Schindler's method delivers K_I as a function of depth directly from the measured strains without first solving for the residual stresses. In addition, it is a surprisingly simple calculation, easily implemented on a spreadsheet. Some additional effort, making use of the weight function, reveals the residual stress profile.

This paper develops and verifies the necessary equations to measure the residual stresses and the resulting stress intensity factor through the remaining ligament of a CT specimen. A finite element simulation provides a realistic residual stress distribution for a CT specimen preloaded beyond yielding. Additional finite element calculations provide the strains measured at the back face for a successively extended, finite-width slot (not a mathematical crack). These simulated strains are used as input data for the different methods for determining the residual stress profile. Next, the results are used to compare the methods for accuracy and ease of implementation. Finally, by introducing realistic errors into the measured strains, the sensitivities of the various methods to experimental errors are evaluated.

SIMULATION

A finite element simulation of a preloaded CT specimen was chosen as a test case with which the accuracy of the various methods for determining residual stress was evaluated. Two conflicting considerations guided the selection of a test case: an accurately known stress profile and physical realism. Experimental specimens cannot be produced with a residual stress profile known accurately enough to unambiguously compare the different methods. On the other hand, analytical solutions, in which arbitrary (besides

satisfying equilibrium) residual stress profiles are assumed, lack physical reality and may erroneously favor one method. Fortunately, finite element simulations model physical behavior reasonably well and give precisely characterized residual stress profiles. In regard to the choice of configuration, the literature indicated that a CT specimen loaded beyond yield and then unloaded, leaving residual stresses, is a realistic and important test case [11–13,19,20].

Figure 1 shows the standard CT specimen geometry and defines some of the variables used in the analysis. The specimen size in the finite element analysis was $W = 50$ mm, with an initial slot length, a_0 , of 25 mm. Note that the slot length a is measured from the center of the loading holes rather than from the specimen edge.

Figure 2 shows the finite element mesh. Only half of the specimen was modeled because of the inherent symmetry. Approximately 3000 2-D plane strain elements, with fully integrated biquadratic shape functions and 8 nodes, were used for the mesh, resulting in about 19,000 degrees of freedom. The mesh was refined near the crack tip and was constructed to allow simulation of the slot cutting by removing appropriate elements. The ABAQUS implicit finite element code [21] was used for all the analyses.

Residual stress

The loading on the CT specimen was modeled using rigid elements to simulate a pin with a diameter of $0.24W$ in the loading hole. The pin was displaced 0.25 mm in the negative y direction, transferring load to the CT specimen by contact. This was sufficient to yield the specimen in compression. In a second analysis step, the load was removed, leaving the residual stresses.

The loading and unloading was modeled with constitutive behavior that would give a realistic residual stress distribution. Elastic-plastic or bilinear stress-strain curves have too sharp of a transition from elastic to plastic, which results in unrealistically sharp peaks in the residual stress profile. Therefore, power law strain-hardening was used:

$$\sigma = K(\varepsilon_0 + \varepsilon_p)^n \quad (1)$$

where σ is the stress and ε_p is the plastic strain, see Fig. 3. The constants used were $K = 676.4$ MPa, $\varepsilon_0 = 0.001$, and $n = 0.15$, which resulted in a 0.2% offset yield of about 280 MPa, with hardening to 532 MPa at a plastic strain of 20%. This yield stress and hardening fits within the range observed for some low-carbon mild steels and for some 300 series stainless steels also [22]. The elastic modulus E was taken as 210 GPa and Poisson's ratio ν as 0.3. The usual elastic relations were used for the stresses below yield and for the elastic strain in the yielded region. The ABAQUS finite element calculations used incremental plasticity, the Mises yield surface and the associated flow rule. Nonlinear combined kinematic and isotropic hardening was chosen for its ability to more accurately model reversed loading [21]. The hardening parameters were calculated automatically in ABAQUS from the half-cycle stress-strain data given by Eq. 1.

The loading was selected such that the plastic zone extended about 3 mm from the crack tip, or about 12% of the remaining ligament of the CT specimen. By trial and error it was found that this provided a residual stress distribution similar to those reported in the literature [10,12,19]. With the element size of 0.2 mm near the crack tip, this put about 15 elements in the plastic zone. The reversed yielding plastic zone during unloading was

smaller but still contained about 10 elements. This is sufficient mesh refinement to capture the peaks in the stress distribution [23].

Slot cutting simulation

It was possible to realistically simulate cutting the slot by sequentially removing elements in the finite element model. Experimentally, wire electric discharge machining (EDM), or spark erosion, is the preferred method for machining the slot because it makes a fine slot and cuts very gently. Typically, for cutting slots of lengths several millimeters or greater, one uses a wire about 0.25 mm in diameter, which could leave a slot up to 0.40 mm wide [10,15]. Therefore, in this analysis the machining of the slot was simulated by incrementally removing the first row of elements along the symmetry plane, which corresponded to a slot 0.40 mm wide. This simulated a square-bottomed slot, whereas an actual wire EDM slot will have a semicircular bottom. However, the difference is negligible for the long, narrow slot considered here [24]. For through-thickness residual stress measurements, one might take strain readings at slot length increments from 0.25 mm to 2.0 mm [15]. In this analysis the strains were taken at 0.4 mm increments. The CT specimen was allowed to unload only elastically during the slot cutting, implicitly assuming no Bauschinger effect or other constitutive nonlinearity. This is a reasonable assumption because the residual stresses are only partially relieved by the slot cutting. The Bauschinger effect is generally only significant when the unloading causes a change in the sign of the stresses.

This analysis ignored any residual stresses generated by the EDM process, which is a reasonable assumption for two reasons [24]. First, optimal machining parameters, which

can generally be achieved by using the EDM machine's "finishing mode," will result in minimal induced stresses. Finishing mode refers to cutting parameters chosen to provide an improved surface finish for manufacturing operations. Second, stresses induced during EDM machining minimally affect the strains measured on the back face opposite the cut.

The strains resulting from cutting the slot were manually calculated from nodal displacements. Typically, one might use a strain gauge of 1.6 mm active length. The strains were therefore calculated by using the symmetry condition and the y -displacement of the node on the back face 0.8 mm from the symmetry plane, see Fig. 2. This gives the average strain over the simulated gauge length.

Figure 4 shows the residual stress profile and the strains from cutting the slot generated by the simulation. The strains are also given in Table 1. The residual stresses that would be measured by cutting the slot are those along the outside edge of the slot, $y = 0.2$ mm, so those are the reported values.

RESULTS AND DISCUSSION

Figure 5 shows the residual stresses determined by reducing the simulation data using the three techniques mentioned in the introduction. Each technique is discussed below. The data points on the fracture mechanics curve are the values returned by that analysis, which gives an average stress over a discrete depth range. Data points are used on the series expansion curve to make the plot visually easier to follow.

Beam-bending approximation

The results in Fig. 5 show that the approximate solution derived by Reid [10] and applied several times in the literature [11–13] results in large errors for the residual

stresses. In Reid's approximation, at each depth increment the remaining uncracked ligament is conceptually separated from the cracked portion of the specimen. The resulting force and moment from the released residual stresses in the cracked portion are then applied to the uncracked portion, and simple beam theory gives the strains. Inverting this process gives the residual stresses from the measured strains as

$$\frac{\sigma(a)}{E'} = -\frac{(W-a)\varepsilon'(a)}{2} - \varepsilon(a) + 3(W-a) \int_{a_0}^a \frac{\varepsilon'(x)}{(W-x)} dx \quad (2)$$

where ε is the measured strain; $E' = E/(1-\nu^2)$ for plane strain, as in this analysis; or $E' = E$ for plane stress. This approximation ignores the stress concentration effects of the crack, the additional stiffness provided by the uncracked portion of the specimen, and the free boundaries at the ends of the beam. Clearly, the approximation is poor and can lead to dangerously nonconservative predictions.

Fracture mechanics approach

The fracture mechanics calculations rely on approximating the slot that was introduced to relieve the residual stresses as a mathematical crack. Cheng and Finnie [25] showed that the approximation is valid for a slot with a depth-to-width ratio greater than five, which is satisfied for most of this test. The results in Fig. 5 further support the validity of this approximation.

Calculating the stress intensity factor K_I from the measured strains is surprisingly simple:

$$K_I(a) = \frac{E'}{Z(a)} \frac{d\varepsilon}{da} \quad (3)$$

where $Z(a)$ is the influence function, which depends on the geometry and the location of the strain measurement but *not* on the residual stress distribution. For a standard CT specimen with a crack depth of $a/W \geq 0.5$ and strain measurement taken at the back face directly opposite the cut, Z is given by Schindler [26]:

$$Z(a) = \frac{-2.532}{(W - a)^{3/2}} \quad (4)$$

In fact, Eq. 4 applies in general to rectangular specimens with deep crack, depending on the specimen length but regardless of geometrical details such as loading holes [26]. Equations 3 and 4 are presented without derivation to illustrate the simplicity of the calculation. The Appendix derives the equations and discusses how to obtain $Z(a)$ for other geometries.

Applying Eqs. 3 and 4 to the simulated strains yields the results in Fig. 6. The method used to differentiate the strains is discussed later, in the discussion of sensitivity to errors. Note that the negative K_I indicates that the slot could try to close on itself. However, the finite element results indicated that the slot closed only a small fraction of its 0.40 mm width.

The residual stresses can be determined from the stress intensity factor by using a weight function solution:

$$K_I(a) = \int_{a_0}^a h(x, a) \sigma_y(x) dx \quad (5)$$

where h is the weight function. Weight function solutions are widely available for many geometries [27]. Equation 5 can be solved for the residual stresses by approximating the stress as a constant, σ_j , within each of n intervals, each bounded by a_{n-1} and a_n . This gives the discrete form of Eq. 5 as

$$K_I(a_i) = \sum_{j=1}^i \sigma_j \int_{a_{j-1}}^{a_j} h(x, a_i) dx \quad (6)$$

Considering Eq. 6 sequentially for each interval allows the σ_j to be uniquely determined.

For a CT specimen the weight function is given by Fett and Munz [27] as

$$h(x, a) = \sqrt{\frac{2}{\pi a}} \frac{1}{\sqrt{1-x/a}} \left[1 + \frac{1}{(1-a/W)^{3/2}} \sum_{v,\mu} A_{v\mu} (a/W)^\mu (1-x/a)^{v+1} \right] \quad (7)$$

where the coefficients $A_{v\mu}$ are those listed in Table 2. Note from Eq. 7 that the integrand in Eq. 6 will be singular for $j = i$ at the $x = a$ endpoint of the interval. This type of singularity can be accurately integrated using numerical quadrature, although the convergence will be somewhat slow [28]. Therefore, Eq. 6 was integrated numerically in this study by using Gaussian integration with four points for the nonsingular intervals and 50 points for the singular intervals, which was found to be sufficiently converged. Applying Eqs. 6 and 7 to the simulated data provided the residual stresses plotted in Fig. 5. The agreement with the known stress distribution is very good.

Series expansion method

In the series expansion implementation of the crack compliance method, the residual stress profile is determined from the measured strains with a technique originally developed for hole-drilling measurements of residual stress [29]. First, the unknown residual stresses are written as a series expansion:

$$\sigma_y(x) = \sum_{i=0}^n A_i P_i(x) \quad (8)$$

where the A_i are unknown coefficients and the P_i are terms in a series: usually polynomials, although any continuous, bounded functions may be used. Then, the strain

that would be measured at the strain gauge location is calculated for each P_i . These strains as a function of depth are called the compliances C_i . Using superposition, one can write the strains for the stress given by Eq. 8 as

$$\varepsilon_y(x) = \sum_{i=0}^n A_i C_i(x) \quad (9)$$

Finally, a least-squares fit is performed between the measured strains and those given by Eq. 9, resulting in the coefficients A_i and, hence, the stresses from Eq. 8.

Legendre polynomials were chosen for the P_i in Eq. 8 because, when the uniform and linear terms are set to zero, such a series will automatically satisfy force and moment equilibrium. Legendre polynomials are the most common choice for through-thickness measurements [15].

The compliances for the CT specimen were calculated using the same finite element mesh used to simulate the residual stress. Starting from a stress-free state, elements were sequentially removed to simulate a slot 0.40 mm wide. For each slot depth and each term in the Legendre polynomial series, Bueckner's superposition principle [30] was used to calculate the strains. The original residual stress variation, with the sign changed, was applied as a pressure load to the face of the slot.

Figure 5 shows the results for a Legendre series expansion of order $n = 9$, with the 0th (uniform) and 1st (linear) order terms set to zero, leaving eight terms. The root-mean-square error between the measured strains and those given by the expansion, Eq. 9, was $2.4 \mu\varepsilon$, which is reasonable but indicates that a different choice of basis function or more terms in the series could result in a better fit.

Ideal case results

Because the results in Fig. 5 were generated with the precise, simulated strain values, they can be used to discuss the best achievable results from each method. Clearly, the beam-bending approximation cannot reproduce the actual residual stress distribution to an acceptable level of accuracy. Unfortunately, this means that the results presented by Reid, Moffatt, and Hermann [11–13] are significantly inaccurate. Both the fracture mechanics approach and the series expansion method give excellent results.

Figure 5 might lead one to erroneously conclude that none of the slot-cutting techniques can accurately resolve the residual stress peak at $x \approx 25.3$ mm. There are two reasons why the peak was not resolved in this simulation. First, a large variation in the stress profile exists in the first 0.5 mm of slot depth. Since strain readings were taken only every 0.4 mm of depth, the variation cannot be resolved. However, the results could easily be improved by using smaller depth increments, which is commonly done [15]. Second, the strain readings were taken at the back face, far from the initial crack tip. An additional strain reading could easily be taken near the crack tip and used to determine the stresses in that area. For the series expansion approach, the compliances (C_i in Eq. 9) for such a location are already available from the same finite element calculation used to compute the compliances for a back-face gauge. For the fracture mechanics approach, a new $Z(a)$ would be needed. In addition, the slot could not be accurately approximated as a crack for depths less than five times the width [25].

The results from the fracture mechanics approach deviate from the known stresses as the cut approaches the back face. This deviation is not a concern in this study primarily because the residual stress and K_I are generally not of interest for very deep cracks since

fatigue or fracture tests are not taken to such depths. In addition, the crack compliance method cannot generally be used for determining the stresses over the last few percent of the specimen thickness because the weight of the specimen and yielding will affect the strain readings [15].

Regardless of the unimportance of the errors for very deep cuts, the reasons for the errors in the fracture mechanics results should be presented for the sake of other applications. The weight function solution is only accurate to a depth of about $a/W = 0.8$ [27]. This is common for weight function solutions because greater depths are rarely of interest. Schindler [16] has developed a correction for very deep cracks, but applying it to this simulation did not result in significantly improved results. Even if a weight function valid for very deep cracks was used, the approximation of the slot as a crack becomes increasingly inaccurate as the cut approaches the back face. The series expansion results do not reflect either of these problems because of the finite element model used to calculate the compliances.

Effect of measurement noise and error

The sensitivity to measurement noise and error is an important consideration for any experimental technique. Even under the best conditions, this type of strain measurement can be expected to have random noise of ± 1 to $2 \mu\epsilon$ [15]. In addition, systematic errors can occur in many forms, such as electronic errors, gauge mispositioning or misalignment, local yielding, and temperature changes. The tolerance to errors of the data reduction techniques can be evaluated by using three types of simulated errors. Adding random noise to the simulated strains simulates experimental noise, adding a

constant value simulates systematic error, and adding values that increase linearly with depth simulates gauge drift or gauge calibration factor error.

In order to fairly compare the sensitivity to errors, the zero data point (depth = 24.65 mm; strain = 0) is kept at zero when noise is added to the strain data. Since the zero point is not included explicitly in the series expansion solution, there is no way to change this assumption. For the fracture mechanics solution, the zero point is used to calculate the strain derivative (see Eq. 3) for the first few points. In fact, for the case of a constant offset added to the strains, the results would not change at all if the zero point were also shifted by the same amount, since only the derivative of strain is used.

The technique used to differentiate the measured strains technique is crucial to the error sensitivity of the fracture mechanics approach. It is well known that differentiation of experimental data can amplify the noise or errors. For this reason, two techniques of differentiating the data were evaluated. The first was to use a four-point smoothing differential:

$$dg(n) = [g(n-2) - 8g(n-1) + 8g(n+1) - g(n+2)]/12 \quad (10)$$

where $g(n)$ refers to the n th data point. This technique was chosen because it is extremely simple to implement. However, it requires evenly spaced data, which is not always the optimal way to take the data [15]. In addition, it cannot be applied to the first two and the last two data points because there are not two data points on either side. Therefore, for the second and the second-to-last data points, the slopes were given from the straight line between the points on either side. For the first and last data points, the slopes were determined by using an exact quadratic interpolation through the three endpoints [31].

The second technique for differentiating the measured strains was a cubic smoothing spline implemented in the MATLAB software [32]. The spline approach is more complicated than simple point-by-point differentiation, but it offers increased control of smoothing and can accommodate unevenly spaced data. The amount of smoothing in the spline is controlled by the parameter p , with $p = 0$ being a straight-line fit through all the data and $p = 1$ being an exact piecewise cubic interpolation (no smoothing). The interesting range of p for smoothing noisy data is in the area of $p = 1/(1+\delta)$, where $\delta = l^3/16$ and l is the average distance between the data abscissae [33]. The results are reported here for two values of the smoothing parameter, $p = 1/(1+\delta)$ and $p = 1/(1+10\delta)$, which work out to about 0.996 and 0.96, respectively, for our data spacing of 0.4 mm. In addition, the spline fit was forced through the first (zero) data point by weighting it 100 times more than the other points in the spline fit. This weighting greatly improved the slopes and the resulting residual stress profile in the high-gradient region near the initial notch tip.

In order to compare the ability of the various methods to determine the correct residual stress profile, a root-mean-square average of the stress error was used. In the fracture mechanics method, the stresses are determined at the midpoint of each depth interval. In the series expansion technique, the stresses are evaluated at the end points of the intervals. The differences between the stresses provided by these techniques and the “known” finite element results are then root-mean-square averaged over all of these points for a single value representing the accuracy of the result. For the evaluation of the random errors, the calculations were repeated with 100 computer-generated random sets at each error magnitude in order to get a converged value of the root-mean-square error.

Figure 7 shows the stress errors that were generated by introducing random errors into the strain data. As expected, the least squares fit used in the series expansion method virtually eliminates the effects of random errors. A large enough value of the smoothing parameter in the spline fit also resulted in good tolerance of random strain errors but at the expense of some accuracy. Less smoothing in the spline gave improved accuracy for low-error strain data but increased the sensitivity to errors. Somewhat surprisingly, the simple four-point numerical differentiation of the strain data gave excellent results. The results would not be quite as good without the previously described modification to the four-point formula for data points near the end of the strain series. Overall, the tolerance of all these methods to a reasonable amount of noise in the strain data, say 3 to 4 $\mu\epsilon$, is excellent.

Figure 8 shows the stress errors for systematic errors introduced into the strain data. The stress errors depend on the sign of the strain errors and even improve the results in some cases because of some fortuitously improved results in the high-gradient region near the original notch tip. The four-point differentiation and close spline fit are the most sensitive to systematic errors, as evidenced by the larger slopes. As previously mentioned, if the zero point were not fixed, the fracture mechanics method would show no sensitivity to a systematic error because it uses only the derivative of strain. Again, the overall tolerance of these methods to errors in the strain reading is very good.

The stress errors for strain gauge drift are not plotted because they are so small for all of the data reduction methods. The simulated strain errors were varied linearly from zero to a maximum value at the final slot depth. Even with the maximum error reaching

$\pm 40 \mu\epsilon$, the resulting root-mean-square stress errors never changed by more than 2 MPa from the error-free results.

Other measurement techniques

It would be difficult to measure the residual stress profile in this study with other established techniques. Hole drilling cannot measure over such a depth range, and it would be virtually impossible to drill the necessary hole near the notch tip. X-rays could only measure the surface stresses on the side of the specimen, which could easily be different from those through the thickness. Neutron diffraction could be used, assuming that the material is crystalline, and would be nondestructive. However, neutrons generally cannot match the spatial resolution of the crack compliance method, and obtaining beam time at a neutron source can be difficult, inconvenient, and time consuming. Sectioning methods could potentially measure the profile, but they have poorer spatial resolution and are experimentally more difficult.

CONCLUSIONS

The crack compliance method has been shown to be a powerful tool for measuring residual stress in a compact tension specimen. Several techniques for implementing crack compliance have been evaluated. The beam-bending approximation of Reid [10] is significantly inaccurate and should not be used. Both the series expansion approach and the fracture mechanics approach work very well, but they offer unique advantages. The following conclusions apply to the fracture mechanics approach:

1. It is the preferred method for determining the stress intensity factor because it is not necessary to first get the residual stresses. The calculation is extremely

simple, especially if a solution for $Z(a)$ already exists for the combination of specimen geometry and strain gauge location.

2. The residual stress results are generally accurate except for very deep cracks.

The calculations require a weight function solution for the given geometry.

3. Because the calculation requires differentiation of measured strains, care must be taken to minimize errors.

4. Because it assumes a mathematical crack, errors result for near-surface measurements where the ratio of slot depth to width is less than about five. Although this was not a concern for the specimen in this study, it should be taken into account for near-surface measurements.

The following conclusions apply to the series expansion approach:

1. The residual stress profile can be determined quite accurately, with some limitations depending on the choice of basis functions.
2. It is very versatile, especially if the compliances are calculated by using a finite element analysis. It is simple to account for the finite width slot, which allows for near-surface measurements, and to get compliances for multiple, arbitrary strain gauge locations.
3. It is especially tolerant to strain measurement errors.

These approaches also offer an exciting possibility for fracture or fatigue tests. By measuring back face strains during machining of the original notch, one could determine the stress intensity factor at the notch tip resulting from residual stresses originally present in the material.

ACKNOWLEDGMENTS

This work was performed at Los Alamos National Laboratory, operated by the University of California for the U.S. Department of Energy under contact number W-7405-ENG-36.

The author thanks Kimberly Becker, who assisted in some earlier finite element calculations on CT specimens.

APPENDIX

Equation 3 in the text can be easily derived. Consider the change in strain energy for extending a crack from a_0 to a in a residual stress field:

$$U = \frac{B}{E'} \int_{a_0}^a [K_{Irs}(a) + K_{IF}(a)]^2 da \quad (A1)$$

where B is the out-of-plane dimension of the specimen, K_{Irs} is the stress intensity factor caused by the residual stresses, and K_{IF} is the stress intensity factor for a pair of virtual forces F at the location and direction of strain measurement. For simplicity, only the mode I stress intensity factor is considered here. Applying Castigliano's theorem yields

$$\delta_F = \frac{1}{2} \frac{\partial U}{\partial F} \Big|_{F=0} = \frac{B}{E'} \int_{a_0}^a K_{Irs}(a) \frac{\partial K_{IF}(a)}{\partial F} da \Big|_{F=0} \quad (A2)$$

where δ_F is the displacement of one of the virtual forces. Considering that K_{IF} is linearly proportional to F and then differentiating by the distance s between the virtual forces gives the strain:

$$\varepsilon = \frac{B}{FE'} \int_{a_0}^a K_{Irs}(a) \frac{\partial K_{IF}(a)}{\partial s} da \quad (A3)$$

where s is usually taken as zero to give strain at a point. Solving for the stress intensity factor gives

$$K_{Irs}(a) = \frac{FE'}{B} \frac{1}{\partial K_{IF}(s) / \partial s} \frac{d\varepsilon(a)}{da} \quad (\text{A4})$$

Comparing the result to Eq. 3 gives

$$Z(a) = \frac{B}{F} \frac{\partial K_{IF}}{\partial s} \quad (\text{A5})$$

As mentioned previously, $Z(a)$ is independent of the residual stress distribution. For solutions for $Z(a)$, see Refs. 16, 17, and 26.

REFERENCES

1. S. J. Maddox (1975) The Effect of Mean Stress on Fatigue Crack Propagation—A Literature Review. *Int. J. Fract.* **11**, 389–408.
2. R. D. Brown and J. Weertman (1978) Mean Stress Effects on Crack-Propagation Rate and Crack Closure in 7050-T76 Aluminum Alloy. *Engng Fract. Mech.* **10**, 757–771.
3. W. O. Soboyejo and J. F. Knott (1990) Effects of Stress Ratio on Fatigue Crack Propagation in QIN (HY80) Pressure-Vessel Steel. *Int. J. Fatigue* **12**, 403–407.
4. K. Tokaji and T. Ogawa (1990) The Effects of Stress Ratio on the Growth Behavior of Small Fatigue Cracks in an Aluminum Alloy 7075-T6 (With Special Interest in Stage I Crack Growth). *Fatigue Fract. Engng Mater. Struct.* **13**, 411–421.
5. A. M. Korsunsky and P. J. Withers (1997) Investigation of Residual Stress Induced Crack Closure and Its Effects on Fatigue in Metal Matrix Composites. *Key Engng Mater.* **127**, 1183–1190.
6. M. Beghini, L. Bertini, and E. Vitale (1994) Fatigue Crack Growth in Residual Stress Fields: Experimental Results and Modelling. *Fatigue Fract. Engng Mater. Struct.* **17**, 1433–1444.
7. C. N. Reid, K. Williams, and R. Hermann (1979) Fatigue in Compression. *Fatigue Engng Mater. Struct.* **1**, 267–270.
8. Y. N. Lenets (1997) Compression Fatigue Crack Growth Behaviour of an Aluminum Alloy: Effect of Overloading. *Fatigue Fract. Engng Mater. Struct.* **20**, 249–256.
9. S. Suresh (1985) Crack Initiation in Cyclic Compression and Its Applications. *Engng Fract. Mech.* **21**, 453–463.

10. C. N. Reid (1988) A Method of Mapping Residual Stress in a Compact Tension Specimen. *Scripta Metall.* **22**, 451–456.
11. C. N. Reid, J. Moffatt, and R. Hermann (1988) Fatigue Under Compressive Loading and Residual Stress. *Scripta Metall.* **22**, 1743–1748.
12. R. Hermann (1994) Fatigue Crack Growth in Ductile Materials Under Cyclic Compressive Loading. *Fatigue Fract. Engng Mater. Struct.* **17**, 93–103.
13. R. Hermann (1995) Crack Growth and Residual Stress in Al-Li Metal Matrix Composites Under Far-Field Cyclic Compression. *J. Mater. Sci.* **30**, 3782–3790.
14. W. Cheng and I. Finnie (1985) A Method for Measurement of Axisymmetric Residual Stresses in Circumferentially Welded Thin-Walled Cylinders. *J. Engng Mater. Technol.* **107**, 181–185.
15. M. B. Prime (1999) Residual Stress Measurement by Successive Extension of a Slot: The Crack Compliance Method. to appear *Appl. Mech. Reviews*.
16. H.-J. Schindler (1995) Determination of Residual Stress Distributions from Measured Stress Intensity Factors. *Int. J. Fract.* **74**, R23–R30.
17. H.-J. Schindler, W. Cheng, and I. Finnie (1997) Experimental Determination of Stress Intensity Factors Due to Residual Stresses. *Exp. Mech.* **37**, 272–277.
18. T. Fett (1987) Bestimmung von Eigenspannungen mittels bruchmechanischer Beziehungen. *Materialprüfung*, **29**, 92-94. For English version see *Engng. Fract. Mech.* **55** (1996), 571–576.
19. J. Smith, M. N. Bassim, C. D. Liu, and T. M. Holden (1997) Measurement of Crack Tip Strains Using Neutron Diffraction. *Engng Fract. Mech.* **52**, 843-851.
20. S. K. Putatunda (1991) Stress Corrosion Crack Growth Behavior of a Low Alloy Steel in 3.0 Percent NaCl Solution. *J. Mater. Engng* **13**, 77-83.
21. ABAQUS/Standard User's Manual Version 5.7. Hibitt, Karlsson & Sorensen, Inc., Pawtucket, Rhode Island, USA (1997).
22. H. E. Boyer, editor (1987) *Atlas of Stress-Strain Curves*, ASM International, Metals Park, Ohio, USA.
23. R. C. McClung and H. Sehitoglu (1989) On the Finite Element Analysis of Fatigue Crack Closure. *Engng Fract. Mech.* **33**, 237-272.
24. W. Cheng, I. Finnie, M. Gremaud, and M. B. Prime (1994) Measurement of Near Surface Residual Stresses Using Electrical Discharge Wire Machining. *J. Engng Mater. Technol.* **116**, 1–7.

25. W. Cheng and I. Finnie (1993) A Comparison of the Strains Due to Edge Cracks and Cuts of Finite Width in a Semi-Infinite Elastic Plate. *J. Engng Mater. Technol.* **115**, 220–226.
26. H.-J. Schindler (1999) Experimental Determination of Crack Closure by the Cut Compliance Technique. To appear in *ASTM STP 1343, Advances in Fatigue Crack Closure Measurement and Analysis*, R. C. McClung and J. C. Newman Jr., editors, American Society for Testing and Materials
27. T. Fett and D. Munz (1997) *Stress Intensity Factors and Weight Functions*. Computational Mechanics Publications, Southampton, UK.
28. P. J. Davis and P. R. Rabinowitz (1984) *Methods of Numerical Integration*, 2nd edition, Academic Press, Orlando, Florida, USA.
29. G. S. Schajer (1981) Application of Finite Element Calculations to Residual Stress Measurements. *J. Engng Mater. Technol.* **103**, 157–163.
30. H.F. Bueckner (1958) The Propagation of Cracks and the Energy of Elastic Deformation. *Trans. Amer. Soc. Mech. Engng*, **80**, 1225-1230.
31. W. H. Press, S. A. Teukolsky, W. T. Vetterling, and B. P. Flannery (1996) *Numerical Recipes in Fortran 77: The Art of Scientific Computing*. Cambridge University Press, Cambridge.
32. MATLAB User's Guide, The MathWorks, Inc., Natick, Massachusetts, USA (1995).
33. C. de Boor (1978) *A Practical Guide to Splines*. Springer Verlag, New York.

a , slot tip position (mm)	Strain ($\mu\epsilon$)	a , slot tip position (mm)	Strain ($\mu\epsilon$)
24.65	0.00	37.4	73.69
25.0	-2.48	37.8	100.59
25.4	-17.91	38.2	129.06
25.8	-41.23	38.6	159.11
26.2	-69.02	39.0	190.69
26.6	-97.70	39.4	223.69
27.0	-124.26	39.8	257.88
27.4	-147.11	40.2	292.89
27.8	-165.83	40.6	328.10
28.2	-180.54	41.0	362.50
28.6	-191.20	41.4	394.48
29.0	-197.69	41.8	421.98
29.4	-199.95	42.2	446.08
29.8	-198.55	42.6	467.54
30.2	-195.00	43.0	486.66
30.6	-189.80	43.4	503.64
31.0	-183.21	43.8	518.58
31.4	-175.38	44.2	531.56
31.8	-166.40	44.6	542.69
32.2	-156.36	45.0	552.00
32.6	-145.31	45.4	559.58
33.0	-133.24	45.8	565.54
33.4	-120.17	46.2	570.01
33.8	-106.08	46.6	573.15
34.2	-90.94	47.0	575.06
34.6	-74.72	47.4	575.89
35.0	-57.37	47.8	575.76
35.4	-38.84	48.2	574.89
35.8	-19.06	48.6	573.59
36.2	2.01	49.0	572.33
36.6	24.45	49.4	571.49
37.0	48.32	49.8	571.19

Table 1. Strains from slot-cutting simulation.

<i>n</i>	<i>m</i>=0	1	2	3	4
0	2.673	-8.604	20.621	-14.635	0.477
1	-3.557	24.9726	-53.398	50.707	-11.837
2	1.230	-8.411	16.957	-12.157	-0.940
3	-0.157	0.954	-1.284	-0.393	1.655

Table 2. Coefficients for CT specimen weight function [27].

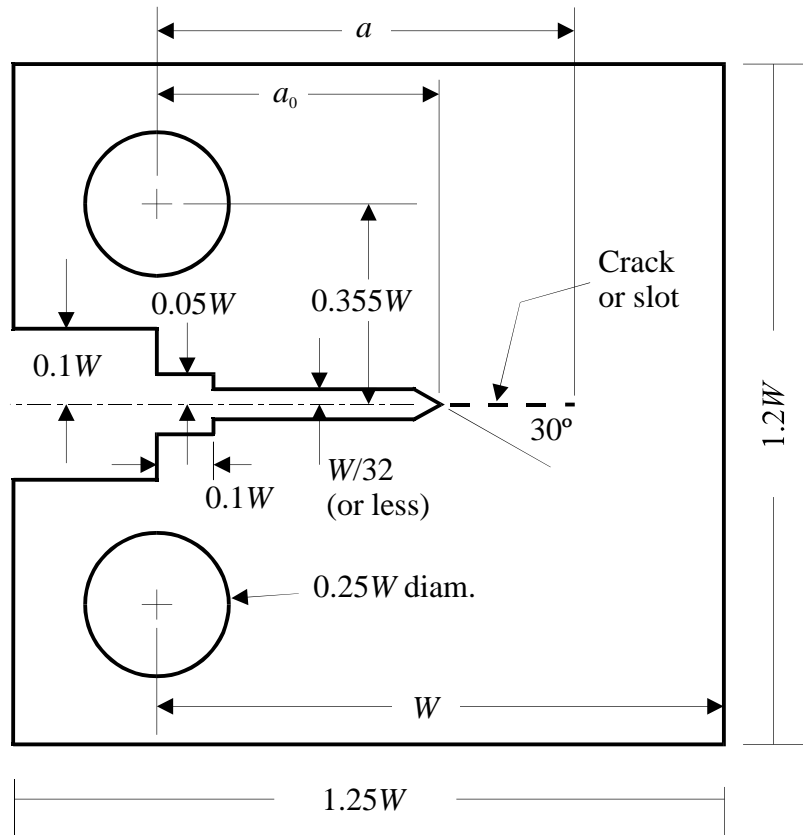


Figure 1. CT specimen geometry.

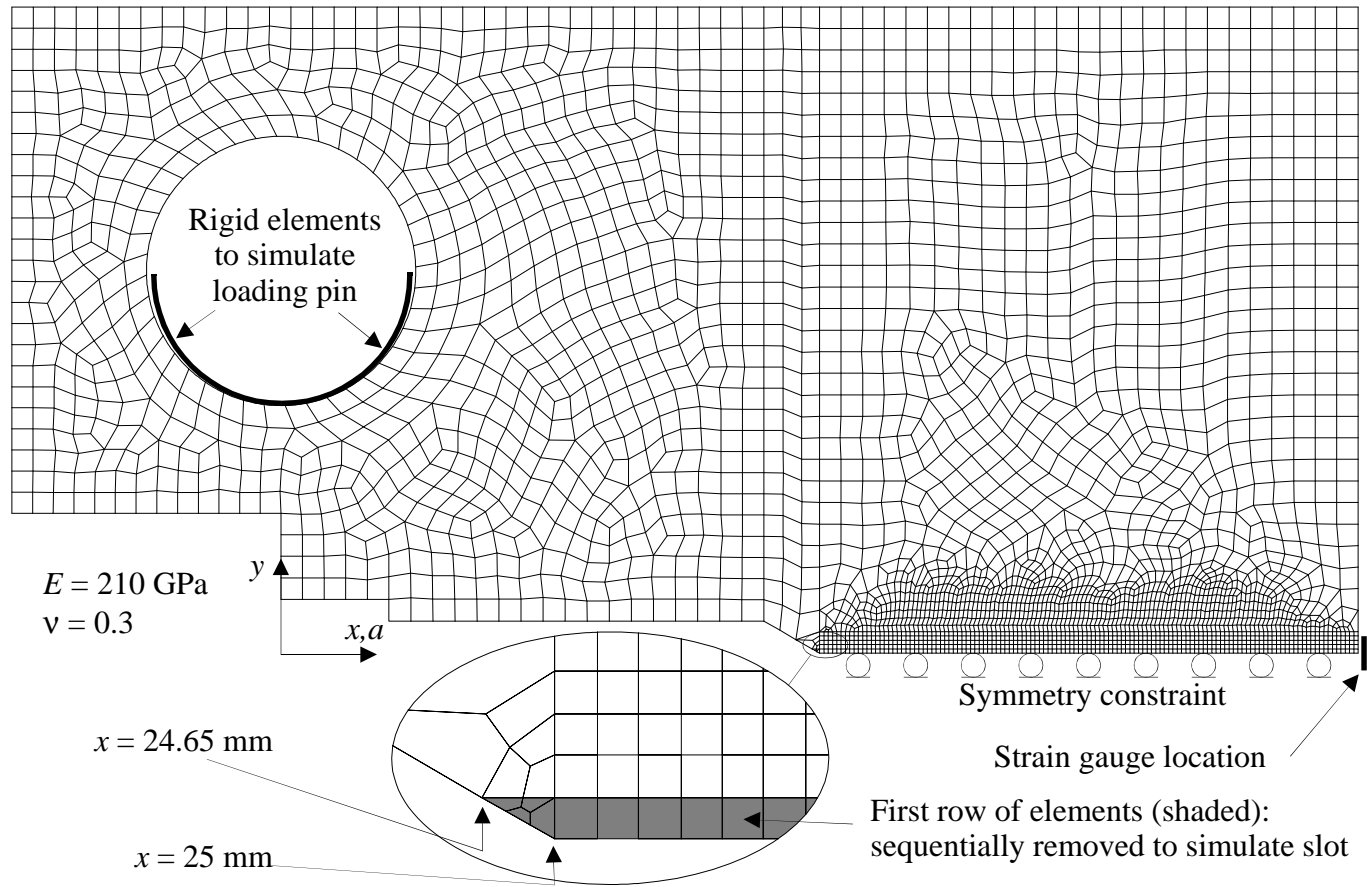


Figure 2. Finite element model of CT specimen.

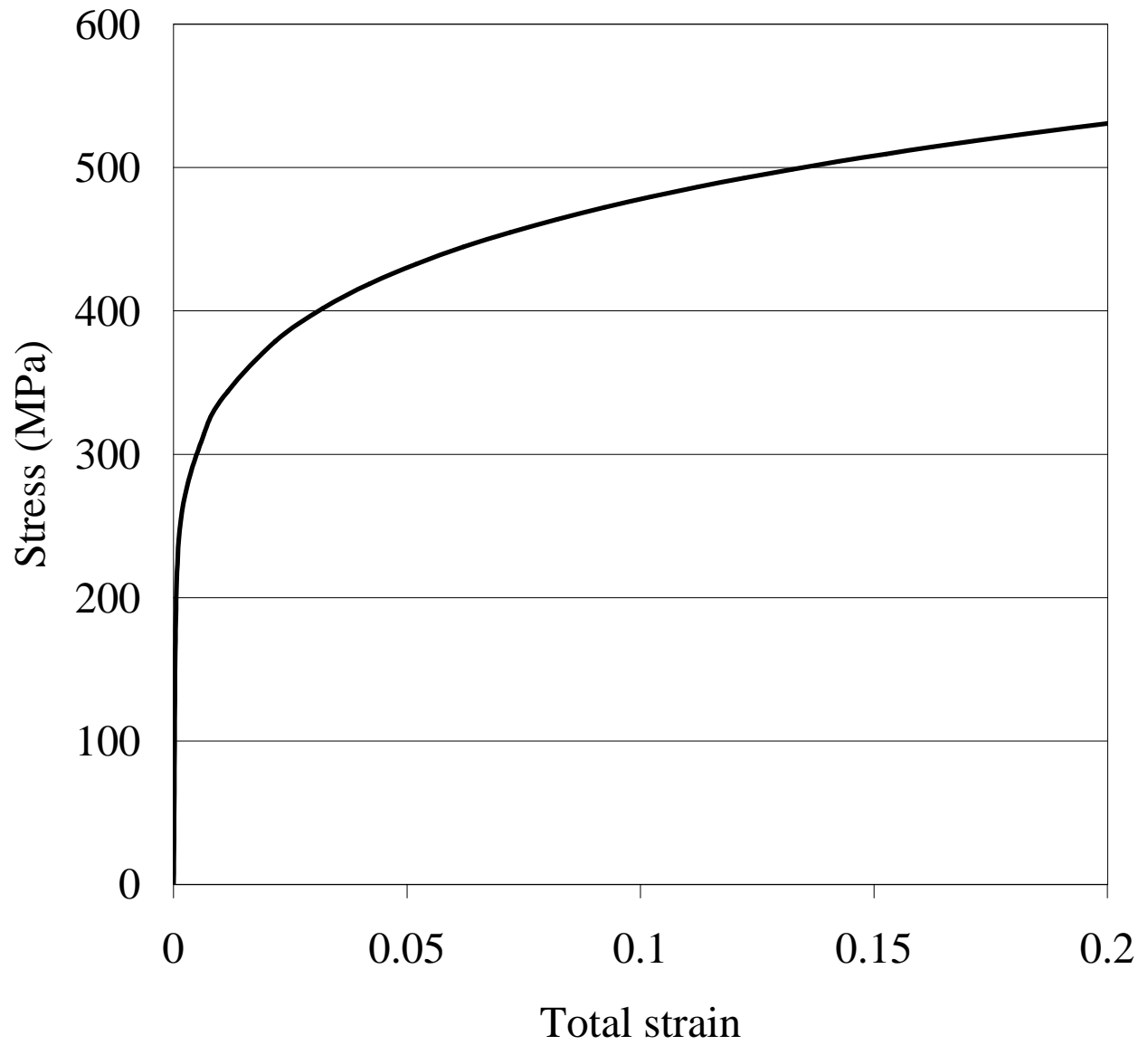


Figure 3. Steel true stress-true strain curve used in simulation.

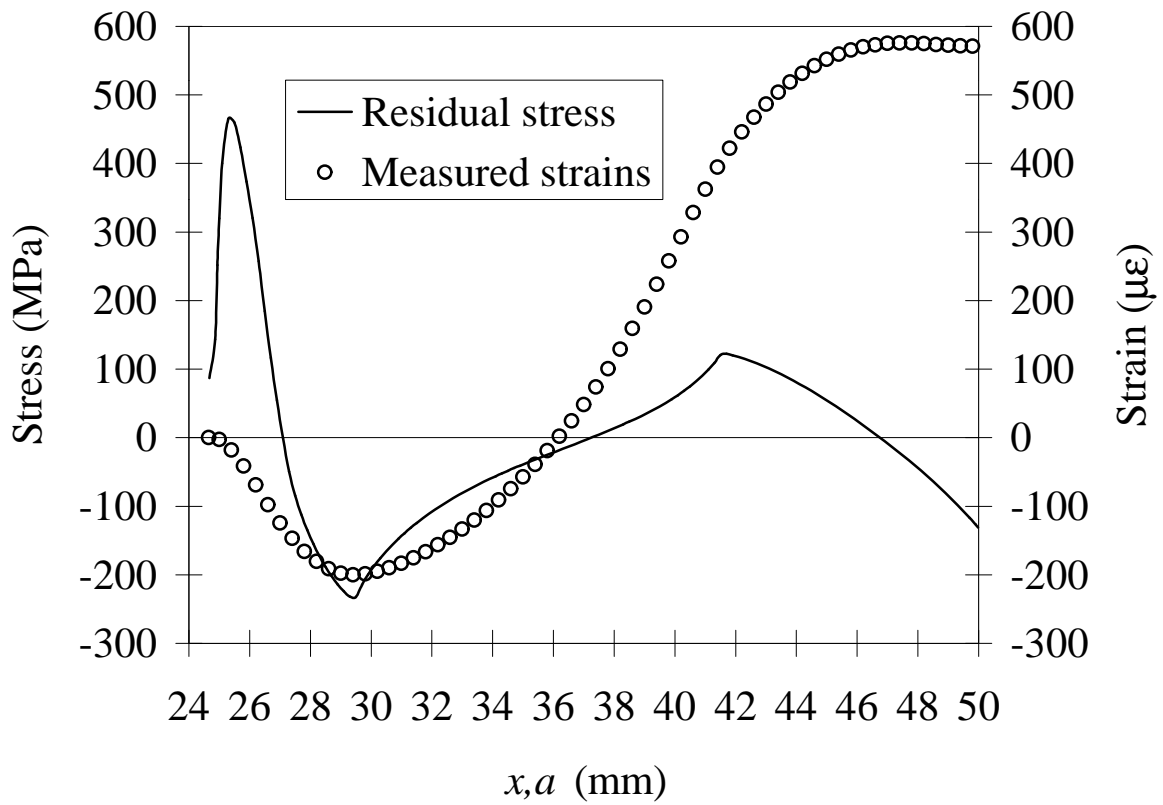


Figure 4. Simulated residual stress profile and simulated strains measured during slot cutting.

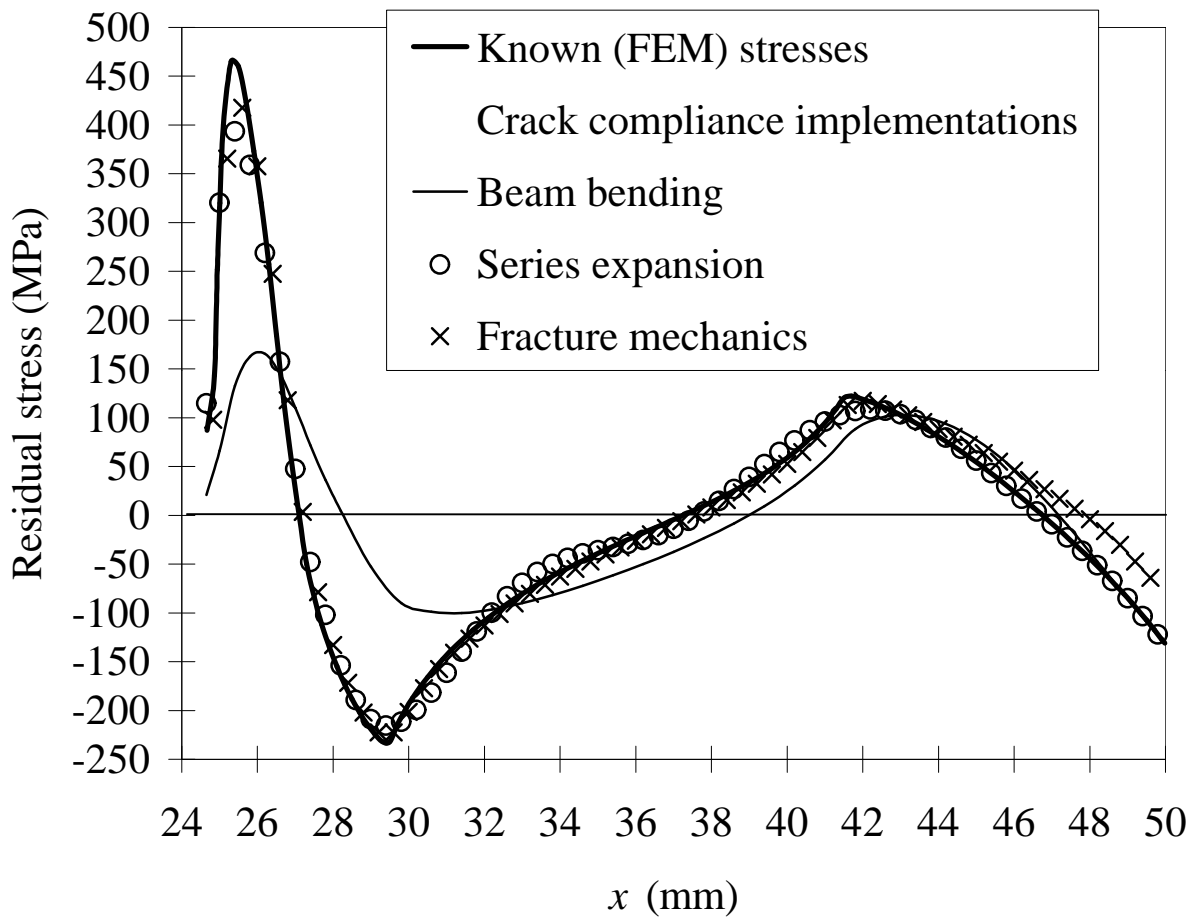


Figure 5. Measured residual stress profiles compared with known finite element distribution.

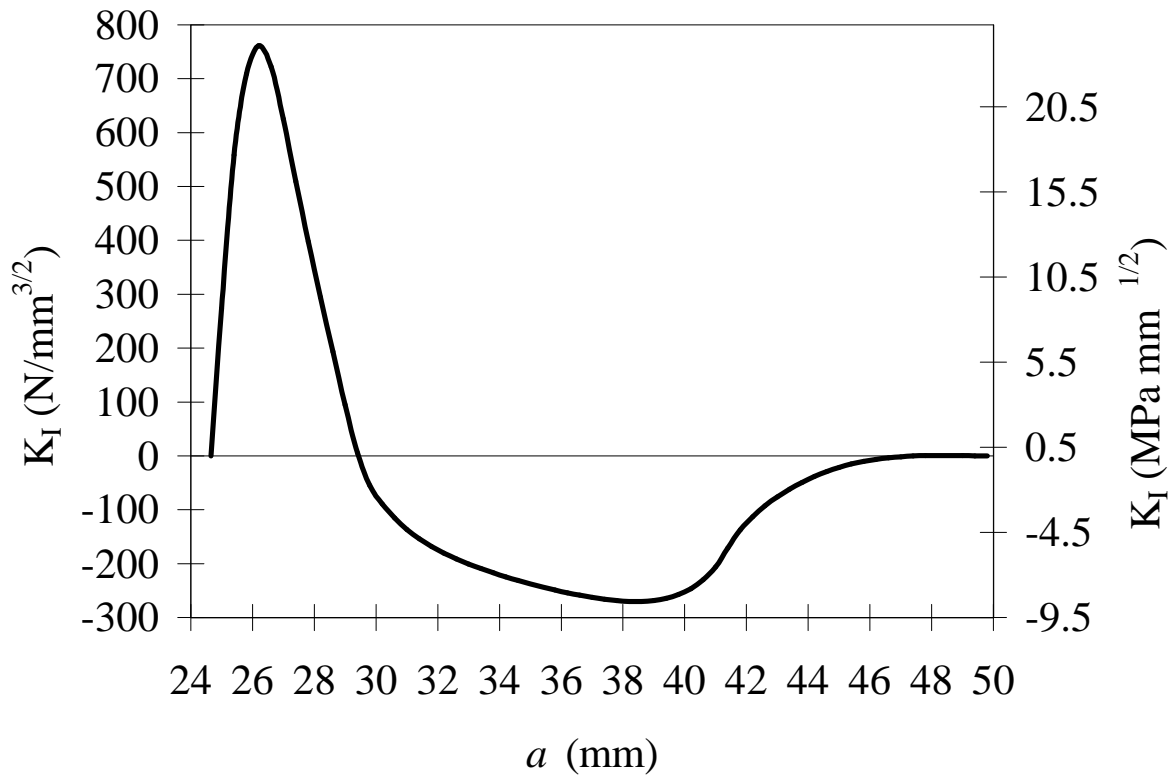


Figure 6. Stress intensity factor for a crack extending into the residual stress field.

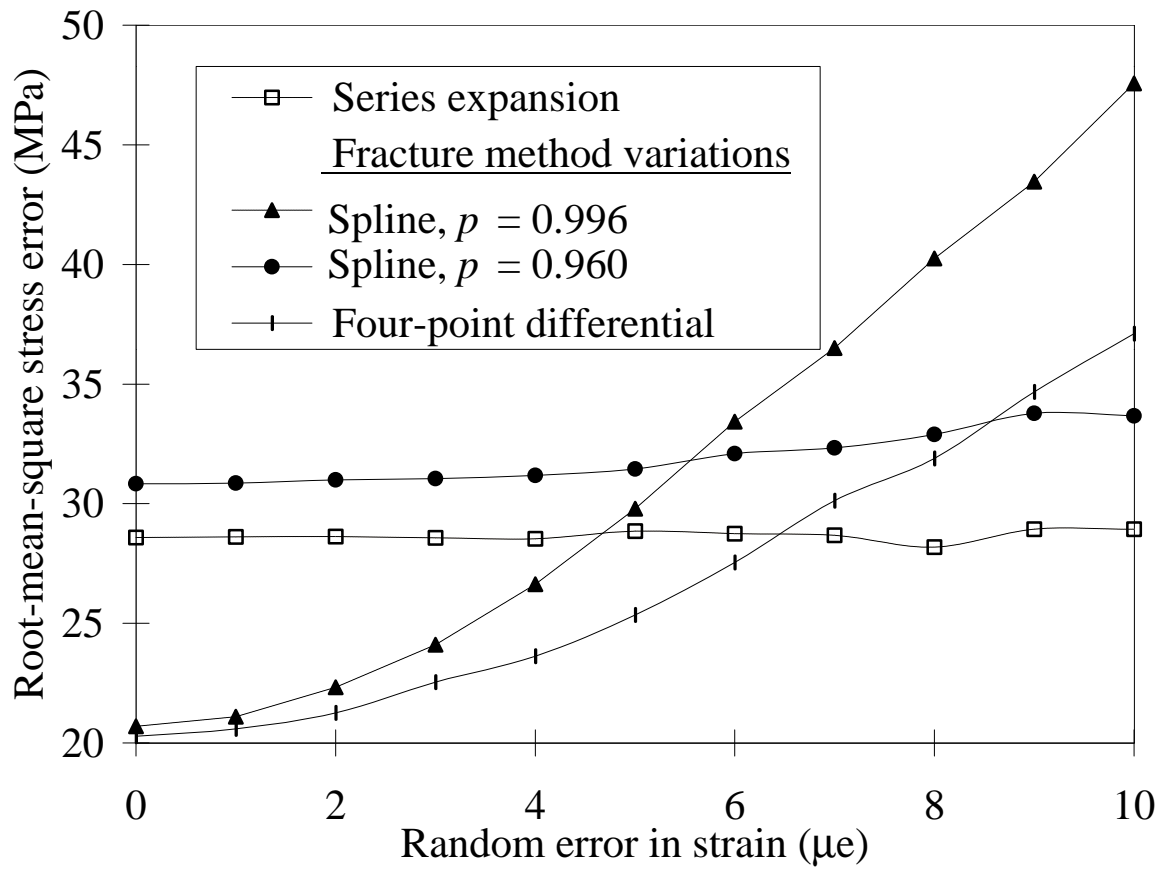


Figure 7. Error in measured residual stress profile caused by random strain errors; p is the spline smoothing parameter.

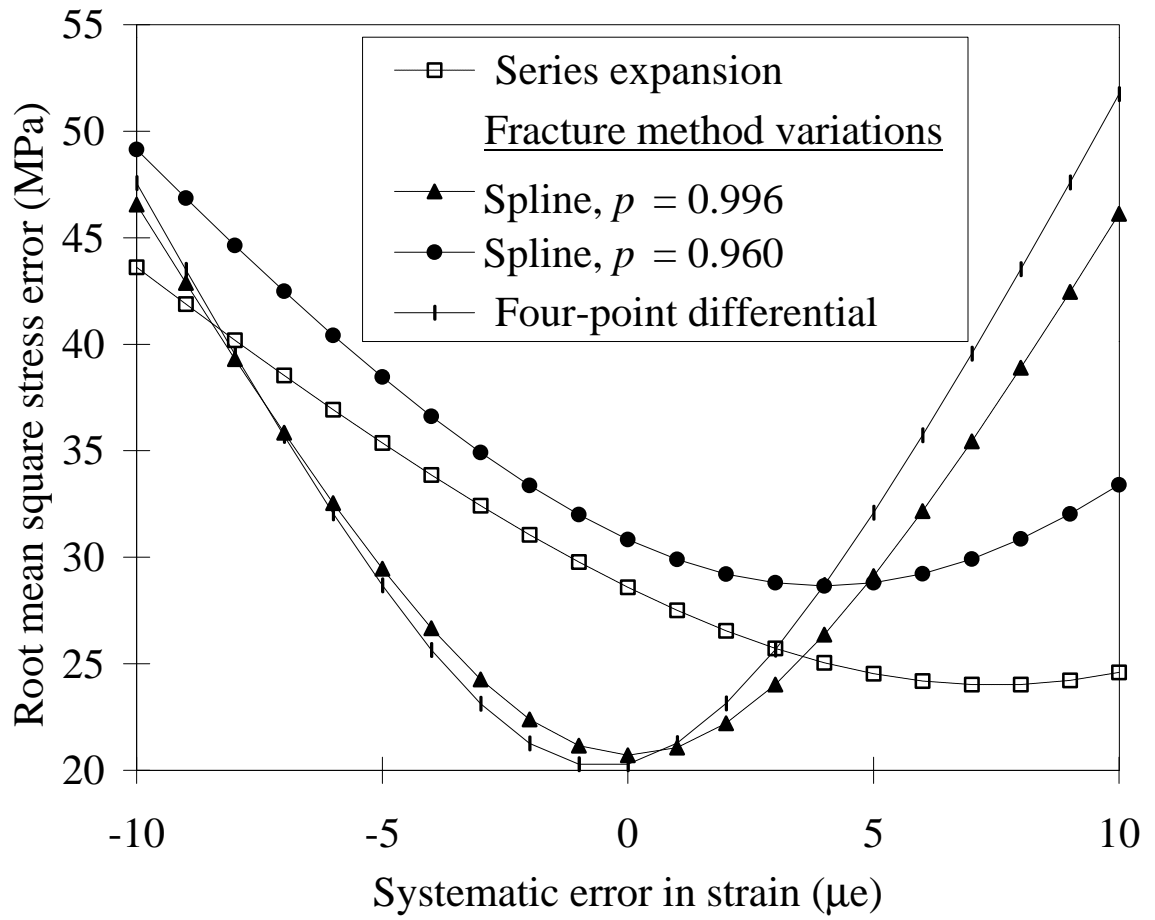


Figure 8. Error in measured residual stress profile caused by systematic strain errors.